CRYSTAL GROWTH & DESIGN
2008
VOL. 8, NO. 5
1774–1778

Synthesis and Gas-Sensing Properties of Pd-Doped SnO_2 Nanocrystals. A Case Study of a General Methodology for Doping Metal Oxide Nanocrystals

Mauro Epifani,*[,†] Jordi Arbiol,[‡,§] Eva Pellicer,[‡] Elisabetta Comini,[||] Pietro Siciliano,[†] Guido Faglia,[||] and Joan R. Morante[‡]

Consiglio Nazionale delle Ricerche - Istituto per la Microelettronica ed i Microsistemi (C.N.R.-I.M.M.), via Monteroni, I-73100 Lecce, Italy, EME/CeAE/IN²UB, Departament d'Electrònica, Universitat de Barcelona, C. Martí i Franquès 1, 08028 barcelona, CAT, Spain, TEM-MAT, Serveis Cientificotècnics, Universitat de Barcelona, C. Lluìs Solè i Sabaris 1, 08028 Barcelona, CAT, Spain, and CNR-INFM and Dip. Chimica e Fisica per l'Ingegneria e i Materiali, SENSOR, Università di Brescia, via Valotti 9, Brescia, Italy

Received October 5, 2007; Revised Manuscript Received February 7, 2008

ABSTRACT: Pd-modified SnO_2 nanocrystals, with a Pd/Sn nominal atomic ratio of 0.025, were prepared by injecting SnO_2 sols and a Pd precursor solution into tetradecene and dodecylamine at 160 °C. Two different doping procedures were investigated: in co-injection, a Pd acetylacetonate solution in chloroform was mixed with the SnO_2 sol before the injection; in sequential injection, the Pd solution was injected separately after the SnO_2 sol. The obtained suspensions were heated at the resulting 80 °C temperature, then the product was collected by centrifugation and dried at 80 °C. When using co-injection, in the dried products PdO and Pd nanoparticles were observed by high-resolution transmission electron microscopy. Only SnO_2 nanocrystals were observed in dried products prepared by sequential injection. After heat-treatment at 500 °C, no Pd species were observed for both doping procedures. Moreover, X-ray photoelectron spectroscopy showed that, in both the doping procedures, after heat-treatment Pd is distributed only *into* the SnO_2 nanocrystal structure. This conclusion was reinforced by the measurement of the electrical properties of Pd-doped nanocrystals, showing a remarkable increase of the electrical resistance if compared with pure SnO_2 nanocrystals. This result was interpreted as Pd insertion as a dopant inside the cassiterite lattice of tin dioxide. The addition of Pd resulted in a remarkable improvement of the gas-sensing properties, allowing the detection of carbon monoxide concentrations below 50 ppm and of very low concentrations (below 25 ppm) of other reducing gases such as ethanol and acetone.

Introduction

The doping of nanocrystalline materials is currently under intensive development, even though many fewer examples are known compared to the synthesis of pure nanocrystals. The inclusion of doping atoms has been of particular interest for the modification of physical properties of the pure nanocrystals and the appearance of new optical[1] or magnetic[2] properties. Recently attention has also been paid to the electrical[3] and gas-sensing properties.[4] The insertion of additives is well-known in the field of gas-sensors for improving sensor properties such as the selectivity and sensitivity.[5] Moreover, the enhancement of gas-sensing properties by using oxide nanocrystals as the sensing layer has already been shown.[6] It is then attractive to study the improvement of the gas-sensing properties due to both the nanomaterials use and their modification with catalytic dopants. The nanocrystal doping in the gas-sensors field is already known,[4,7] but this result is generally obtained by impregnation procedures, which may result in inhomogeneous distribution of the additive. It is then necessary to develop synthetic protocols going beyond the classical impregnation procedure. We have developed a general protocol[8] for the synthesis of oxide nanocrystals, relying on the injection of a metal oxide sol in a coordinating environment, without using extreme processing conditions. In this way, it is easy to conceive process modifications in order to introduce additives into the final nanocrystals. By exploiting these general features of the synthesis, in this work we investigate, as a case study of a general methodology, two different procedures for Pd addition in SnO_2 nanocrystals. Sequential injection or co-injection of the Pd precursor with respect to the injection of the SnO_2 sol were investigated. The two different routes were developed in order to compare the result of Pd addition to preformed nanocrystals or while the latter are simultaneously growing. The Pd-SnO_2 system was chosen as a case study since it is one of the most widespread materials in commercial chemoresistive sensors. Depending on the injection procedure, separate formation of PdO species may be obtained, but upon heat-treatment Pd is present only in the SnO_2 nanocrystals, and strongly influences the electronic properties of the final material. In particular, the resulting sensing devices were very sensitive to CO and other reducing gases, with a detection limit well below the 30 ppm value usually reported for commercial sensors.

Experimental Procedures

a. Sol Preparation. The starting SnO_2 sol was prepared by reacting 3.9 mmol of anhydrous $SnCl_4$ with 10 mL of methanol in a glovebox. After the evolution of vapors had stopped, water was dropped in order to reach a H_2O/Sn molar ratio of 16. The obtained solutions were further stirred for 24 h, which remained clear and colorless.

b. Sol Injections and Processing of Pure SnO_2. In a 500 mL flask, equipped with a thermometer, a condenser, and a rubber septum, 10 mL of tetradecene were mixed with 1 mL of dodecylamine. The flask was degassed with nitrogen and heated up to 160 °C. When the temperature was reached, 2 mL of the previously described SnO_2 sol was injected rapidly through the septum, with the release of a huge amount of vapors. Caution must be taken in this stage to release the eventual vapor pressure while proceeding with the injection. After the

* To whom correspondence should be addressed. E-mail: mauro.epifani@le.imm.cnr.it.
† C.N.R.-I.M.M.
‡ Departament d'Electrònica, Universitat de Barcelona.
§ TEM-MAT, Serveis Cientificotècnics, Universitat de Barcelona.
|| Università di Brescia.

10.1021/cg700970d CCC: $40.75
Published on Web 04/05/2008

injection, the temperature dropped to about 80 °C, and the power supply to the flask heating was decreased in order to keep constant such temperatures. After 3 h since the injection, the flask was removed from the heater and cooled. The resulting white slurries were recovered from the flask, and eventually methanol or isopropanol was added. After centrifugation, a white precipitate was recovered, washed with hexane, and dried in air at 80 °C. Heat-treatments of the dried powders were carried out in air in a muffle furnace at 500 °C for 1 h, with a heating rate of 5 °C/min. Yellow powders were obtained.

c. Sol Injections and Processing of Pd-Modified SnO_2. Two different procedures were employed for preparing Pd-modified SnO_2 nanocrystals, with Pd/Sn nominal atomic ratio equal to 0.025. In the sequential injection procedure, the SnO_2 sol was first injected in the flask. After 1 h and 45 min, the required Pd acetylacetonate ($Pd(acac)_2$) amount dissolved in chloroform was injected in the flask, followed by further heating for 1 h and 15 min. In the coinjection procedure the required amount of $Pd(acac)_2$ dissolved in 1 mL of chloroform was mixed with 2 mL of the SnO_2 sol, and the resulting solution was injected through the septum. The following post-injection processing was then identical to that described for pure SnO_2. The heat-treated powders had a light orange color.

d. Materials Characterization. (i) X-Ray Diffraction (XRD). XRD patterns of the dried or heat-treated powders were obtained with a Siemens D-500 X-ray diffractometer using Cu Kα radiation (λ = 1.5418 Å), with an operating voltage of 40 kV and a current of 30 mA. Data were collected in steps of 0.05° (2θ) from 10° to 80°.

(ii) X-ray Photoelectron Spectroscopy (XPS). XPS spectra were taken with a Perkin-Elmer PHI ESCA-5500 equipment using Al Kα radiation (1486.6 eV). Analyses were done both before and after Ar-ion sputtering for 1 min.

(iii) High-Resolution Transmission Electron Microscopy (HRTEM). The structural and morphological characterization of the samples was carried out by means of transmission electron microscopy (TEM) and selected area electron diffraction (SAED). In order to obtain the high resolution TEM results we used a field emission gun microscope Jeol 2010F, which works at 200 kV and has a point-to-point resolution of 0.19 nm. To improve our images contrast and resolution avoiding the chromatic aberration inherent in HRTEM micrographs, we obtained the images by filtering the electron zero loss peak, using a Gatan Image Filter (GIF). Low magnification images, as well as selected area electron diffraction (SAED) patterns were obtained from a Philips CM30 LaB_6 microscope operated at 300 kV. SAED intensity profiles were quantified by using Process Diffraction software. Electron energy loss spectroscopy (EELS) spectra were obtained in a Gatan Image Filter (GIF 2000) coupled to the Jeol 2010F microscope. Spectra obtained achieved an energy resolution of 1.2 eV.

(e) Processing and Testing of Gas-Sensing Devices. Nanocrystal suspensions were prepared by dispersing 4–6 mg of the as-prepared products in 1–1.5 mL of hexane. Drops of the suspensions (about 4 μL) were deposited onto the substrates and waiting for complete evaporation of the solvent before depositing the next drop. Alumina substrates (2 × 2 mm^2) were used, with predeposited platinum electrodes on the front side and platinum heaters on the back. Gold wires had been bonded to the electrodes and the heaters before the drop-coating step. The flow-through technique was used to test the electrical and gas-sensing properties of the thin films. A constant flux of synthetic air of 0.5 L/min was used as gas carrier into which the desired concentration of CO, acetone or ethanol was mixed. All the measurements were executed in a temperature-stabilized sealed chamber at 20 °C under controlled humidity. Electrical characterization was carried out by volt-amperometric technique; the sensor was biased by 1 V and film resistance was measured by a picoammeter.

Results and Discussion

Materials Synthesis and Characterization. The choice of the Pd precursor was suggested by the need for moderating the reduction rate of Pd^{2+} to Pd^0. The latter may result in uncontrolled Pd precipitation if, for instance, a Pd acetate solution is used as the Pd precursor. It was found that Pd acetylacetonate constitutes a convenient and easily available Pd source. Figure 1 reports the XRD patterns of both the as-obtained, dried nanocrystals and those heat-treated at 500 °C.

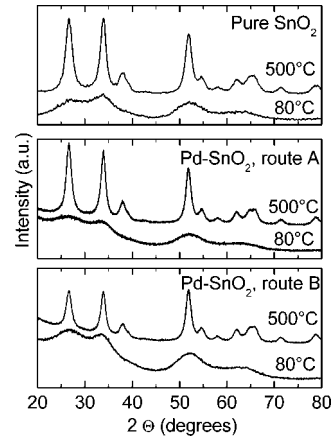

Figure 1. XRD patterns recorded on pure and Pd-modified SnO_2 nanocrystals prepared by sequential injection (route A) and co-injection (route B), respectively.

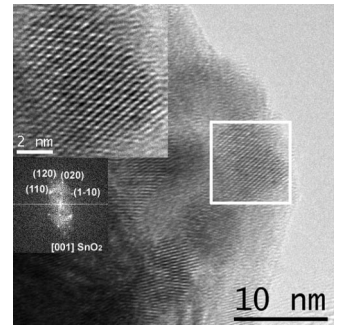

Figure 2. HRTEM image of Pd-SnO_2 nanocrystals, prepared by co-injection and heat-treated at 500 °C. The insets show higher magnification of the selected area and the related power spectra.

Table 1. Mean SnO_2 Nanocrystals Size (nm) Obtained from TEM Images

sample	as-dried	500 °C
pure SNO_2	2.2 ± 0.2	6.0 ± 1.0
sequential injection	2.0 ± 0.3	8.5 ± 2.5
co-injection	1.9 ± 0.3	7.0 ± 1.6

For comparison, the patterns related to pure SnO_2 nanocrystals are reported. In all the patterns only the reflections of the tetragonal phase of SnO_2 are seen.

From the analysis of the peak broadening[9] for the samples heat-treated at 500 °C, it was obtained that Pd addition results in larger SnO_2 nanocrystals, with a size of 7.5 nm with respect to 5.9 nm of pure SnO_2. These conclusions are confirmed by the results of the TEM observations. An example is shown in Figure 2, related to the sample prepared by sequential injection and heat-treated at 500 °C. TEM images related to the other samples are reported in the Supporting Information.

Figure 2 shows tetragonal SnO_2 nanocrystals, with a mean size of 8.5 ± 2.5 nm, larger than the pure SnO_2 nanocrystals, which are characterized by a mean size of 6.0 ± 1.0 nm. The prediction from the XRD patterns are hence confirmed, and a summary of the SnO_2 nanocrystal size, as obtained from TEM observations, is reported in Table 1.

In our previous work,[8] it was found the nanocrystal size is stabilized against growth during the heat-treatment by the presence of a carbon shell originated by the synthesis residuals. Thus a possible explanation for the larger SnO_2 nanocrystal size in Pd-modified samples may involve just the catalytic effect of

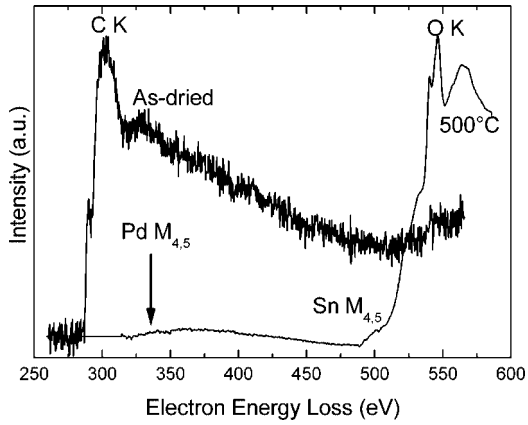

Figure 3. EELS spectra recorded on the indicated samples prepared by sequential injection.

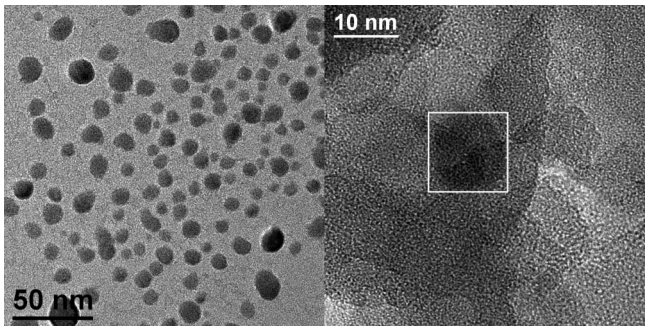

Figure 4. General view of a Pd-enriched region in as-dried, co-injected Pd-SnO_2 sample (left) and magnified detail of one of such regions, showing a Pd nanocrystal (see Figure 5).

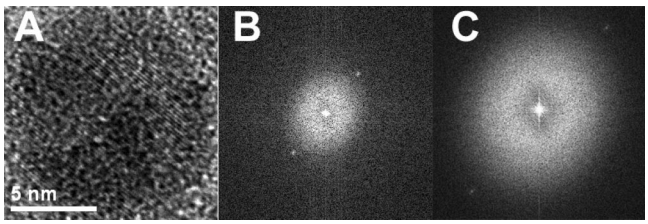

Figure 5. Magnification of the Pd nanocrystal in Figure 4(A), related power spectra, showing the {111}Pd diffraction spots (0.224 nm) (B) and power spectra of the wider region comprising it (C).

Pd toward the oxidation of such shell. The TEM analysis, coupled with electron energy loss spectroscopy (EELS), was also used for determining the presence of palladium and its distribution in the various samples. In samples prepared by sequential injection no evidence of Pd crystalline phases was obtained in the TEM images and from selected area electron diffraction (SAED) pattern analysis. Only by EELS was the presence of Pd accumulation regions observed in the sample heated at 500 °C, where an atomic percentage of Pd of 5% with respect to Sn was detected, as shown in Figure 3.

The situation in the case of co-injection was more peculiar, since in some regions of the dried sample we observed discrete, amorphous particles, characterized by a spheroidal morphology, as shown in Figure 4.

When observing in detail such regions, the sporadic presence of nanocrystals with a size of about 10 nm was found, as shown in Figure 4 and, in detail, in Figure 5A. The corresponding power spectra (Figure 5B) allowed identification of the nanocrystals as elemental Pd. On the other hand, power spectra of the whole area comprising the nanocrystals (Figure 5C) show that it is amorphous. Finally, EELS spectra of this region display the presence of oxygen.

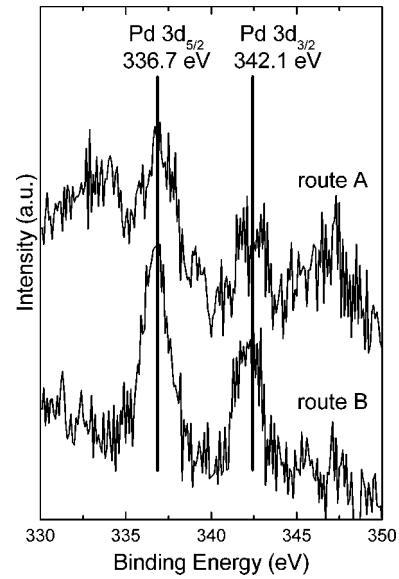

Figure 6. XPS spectra in the Pd 3d region measured on as dried samples prepared by the indicated routes.

So, by a co-injection procedure, it seems favored the formation of regions mainly composed of amorphous palladium oxides, including some Pd nanocrystals, most probably stabilized against oxidation just by the external oxide region. After heat-treating at 500 °C, no discrete Pd species could be observed.

An independent Pd determination was carried out by XPS for all the doping procedures, for gaining information from larger sample areas in comparison to EELS. The surface of the samples did not show any Pd presence, but, after sample sputtering, a weak but clear Pd signal emerged, shown in Figure 6. The binding energy was typical of Pd(II) bonded with oxygen (PdO), so confirming the presence of oxidized palladium. This result holds for samples prepared with both procedures, both as-dried and heat-treated at 500 °C. The survey spectra, shown in the Supporting Information, display a small chlorine concentration that disappears after heat-treatment, similarly to carbon, that is diminished to very small concentrations. No other contaminants were detected. A quantitative determination was not possible due to the weak Pd signal; in any case it appears that the nominal concentration of 2.5% is not present in the final material. This result can be related to the observed segregation effects of Pd, leading to a decrease of the effective Pd concentration in the SnO_2 structure. At this point, it can be concluded that the co-injection procedure favors the formation of discrete PdO species, with some Pd nanocrystals included, but that they are dissolved upon heat-treatment at 500 °C.

On the other hand, sequential injection favors a better initial distribution of Pd in the SnO_2 matrix, with no PdO species observed. The reason for these differences can depend on the different morphology of the SnO_2 species interacting with the Pd species. In the sequential injection procedure, as soon as $Pd(acac)_2$ is decomposed, the resulting Pd species are hindered from forming nanoparticles by the presence of preformed SnO_2 nanoparticles. In the co-injection procedure, if the formation rate of Pd and SnO_2 species are similar, separate nucleation of both nanoparticles may occur. From the XPS results, it seems that the most general feature of the samples is that Pd is

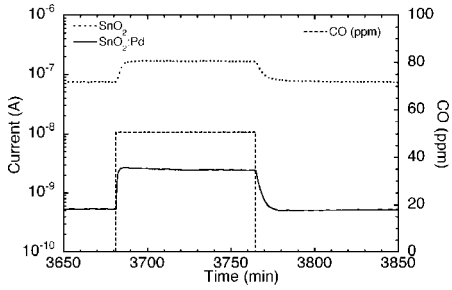

Figure 7. Dynamic response curves for the indicated materials at 300 °C and to a CO concentration of 50 ppm.

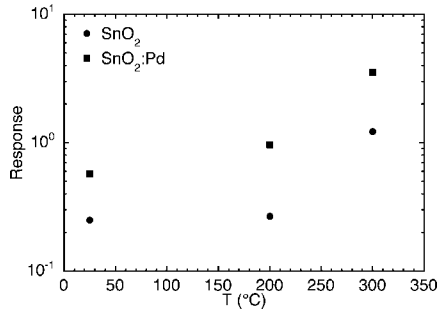

Figure 8. Temperature-response comparison between the indicated nanocrystals for a CO concentration of 50 ppm.

distributed inside the SnO_2 structure (it is observed only after sputtering), while some Pd accumulation regions may be encountered. The preferable procedure is sequential injection, since the initial separate formation of PdO is avoided. This is not to be meant as a general rule, since the decomposition rate of the metal precursor will change depending on the particular metal and on the related ligands, and each time a careful analysis would be needed.

Functional Characterization of Gas-Sensing Devices. Carbon monoxide was chosen as a test gas being one of the most common target gases for Pd-modifed commercial sensors. We only tested the nanocrystals obtained by sequential injection, since the materials prepared by co-injection had a very high electrical resistance.

In Figure 7 the dynamic response curves are reported for both pure and Pd-modified SnO_2nanocrystals based sensors, at a sensor operating temperature of 300 °C and with 50 ppm of CO. The Pd-modified nanocrystals display remarkably improved response and recovery time, which are 85 and 185 s, respectively, against corresponding values of 335 and 295 s for pure SnO_2. Even the response (defined as the relative variation of conductance with respect to the initial value in pure air) is much improved with respect to pure SnO_2. This result is evidenced in Figure 8, where the response is compared for the two materials at various operating temperatures for 50 ppm of CO. The response increase occurs at all temperatures, but an operating temperature of 300 °C is highlighted as the best one by the calibration curves in Figure 9 (the corresponding plot for an operating temperature of 200 °C is reported in the Supporting Information). In fact, the possibility of detecting CO concentrations lower than 30 ppm by the Pd-modified nanocrystals is evident. This is the most remarkable result, since 30 ppm is generally the detection limit of commercial sensors. Results on other reducing gases such as ethanol and acetone are also shown in Figure 9. The enhanced response properties of Pd-SnO_2 nanocrystals are further evidenced: very high

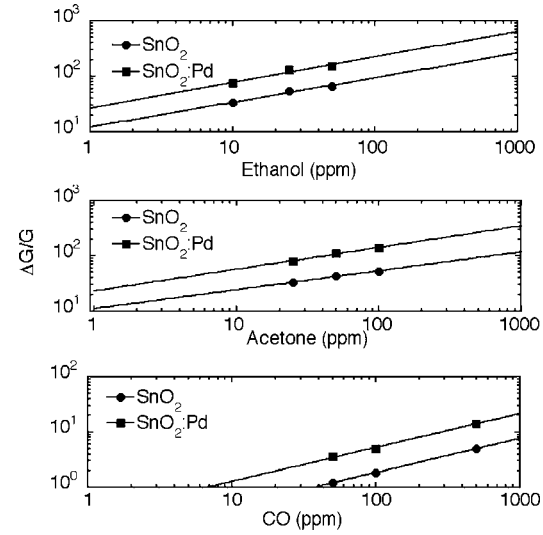

Figure 9. Calibration curves for CO sensing for the indicated materials at an operating temperature of 300 °C.

responses are obtained even for as low as 10 ppm and 25 ppm concentrations, providing the potential of detecting gas concentrations down to 1 ppm.

The dynamic response curves and the temperature-response curves for the lowest concentrations used in the tests are reported in the Supporting Information, for completeness. The positive effect of catalyst introduction on the sensor performances is clear and deserves specific considerations. In general, the beneficial effect on the sensor performance by noble metal catalysts is attributed to different kinds of sensitizations: chemical sensitization occurs by spill-over of active species, generated by the interaction with the catalyst, over the sensor surface. For instance, Pd nanoparticles (in particular, PdO) may generate active oxygen species which are then distributed over the surrounding sensor surface, increasing its resistance and hence improving the response to reducing gases. On the other hand, electronic sensitization reflects direct reactions of the catalyst with the gaseous analyte. For instance, electron flow may initially occur from the semiconducting sensing material to the Pd catalyst, again increasing the sensor resistance, which is recovered after reaction of Pd with the reducing gases.

In our materials we could not detect discrete Pd or PdO nanoparticles decorating the SnO_2 nanocrystals. Moreover, the XPS results further reinforce the hypothesis of Pd distributed *into* the SnO_2 structure. For these reasons, we *cannot* invoke classical sensitization mechanisms for explaining the improved sensing performances of the Pd-modified SnO_2 nanocrystals. Assuming sensitization effects is simplistic, without a detailed knowledge of the additive distribution in the oxide structure. Instead, the influence of the additive on the electronic properties of the oxide must be considered, and such influence, in our case, is clearly shown by the decrease of the sensor base resistance when Pd is present. From XPS, Pd is present as Pd(II) into the nanocrystal structure, and the resistance decrease can be explained by a p-doping effect by Pd(II) into the SnO_2 structure. Thus Pd doping would compensate the free carriers generated by oxygen vacancies, which typically provide the n-type feature of tin dioxide. It is not yet clear in which way the sensing properties are consequently improved, but our interpretation of Pd influence is in full agreement with, for instance, ref 5e. The authors showed that the modification of the oxide electronic structure by the catalyst should be kept into account in a general model explaining the improvement of the sensing properties.

The gas-sensing results in the present work indeed show that a proper insertion of a catalyst in the oxide structure may result in a strong improvement of the sensing properties.

Conclusions

The synthesis of SnO_2 nanocrystals by injection of metal oxide sols in a coordinating environment allowed easy modification of the preparation protocol in order to introduce Pd in the nanocrystal structure. Depending on whether Pd is introduced by co-injection or sequential injection, separate Pd or PdO species are occasionally encountered in the final materials, but the general feature of the materials is constituted by SnO_2 nanocrystals incorporating Pd in the form of oxidized species. This material composition gives rise to lower base currents, but at the same time provides much enhanced gas-sensing properties, which have been interpreted as a modification of the electronic structure of SnO_2, since classical sensitization mechanisms cannot be invoked. In particular, concentrations of CO, ethanol, and acetone below 30, 10, and 25 ppm, respectively, can be detected by the Pd-SnO_2 nanocrystals.

Acknowledgment. The authors thank the XRD and XPS units of the Serveis Científico-Tècnics of the University of Barcelona for their cooperation. This work was supported by the European Union in the frame of the NANOS4 (Grant NMP4-CT-2003-001528) project.

Supporting Information Available: Further HRTEM images of as-dried and heat-treated samples, XPS survey, dynamic response curves for tests to acetone and ethanol). This material is available free of charge via the Internet at http://pubs.acs.org.

References

(1) (a) Mikulec, F. V.; Kuno, M.; Bennati, D. A; Hall, D. A.; Griffin, R. G.; Bawendi, M. G. *J. Am. Chem. Soc.* **2000**, *122*, 2532–2540. (b) Raola, O. E.; Strouse, G. F. *Nano Lett.* **2002**, *2*, 1443–1447. (c) Stowell, C. A.; Wiacek, R. J.; Saunders, A. E.; Korgel, B. A. *Nano Lett.* **2003**, *3*, 1441–1447. (d) Wang, X.; Kong, X.; Shan, G.; Yu, Y.; Sun, Y.; Feng, L.; Chao, K.; Lu, S.; Li, Y. *J. Phys. Chem. B* **2004**, *108*, 18408–18413. (e) Heer, S.; Kömpe, K.; Güdel, H.-U.; Haase, M. *Adv. Mater.* **2004**, *16*, 2102–2105. (f) Pradhan, N.; Goorskey, D.; Thessing, J.; Peng, X. *J. Am. Chem. Soc.* **2005**, *127*, 17586–17587. (g) Sapra, S.; Prakash, A.; Ghangrekar, A.; Periasamy, N.; Sarma, D. D. *J. Phys. Chem. B* **2005**, *109*, 1663–1668. (h) Viswanatha, R.; Chakraborty, S.; Basu, S.; Sarma, D. D. *J. Phys. Chem. B* **2006**, *110*, 22310–22312. (i) Pellegrino, P.; Garrido, B.; Arbiol, J.; Garcia, C.; Lebour, Y.; Morante, J. R. *Appl. Phys. Lett.* **2006**, *88*, 121915/1-3. (j) Pradhan, N.; Battaglia, D. M.; Liu, Y.; Peng, X. *Nano Lett.* **2007**, *7*, 312–317.

(2) (a) Bryan, J. D.; Heald, S. M.; Chambers, S. A.; Gamelin, D. R. *J. Am. Chem. Soc.* **2004**, *126*, 11640–11647. (b) Bryan, J. D.; Santangelo, S. A.; Keveren, S. C.; Gamelin, D. R. *J. Am. Chem. Soc.* **2005**, *127*, 15568–15574. (c) Archer, P. I.; Radovanovic, P. V.; Heald, S. M.; Gamelin, D. R. *J. Am. Chem. Soc.* **2005**, *127*, 14479–14487. (d) Martínez, B.; Sandiumenge, F.; Balcells, Ll.; Arbiol, J.; Sibieude, F.; Monty, C. *Phys. Rev. B* **2005**, *72*, 165202/1–165202/8. (e) Pan, D.; Wan, J.; Xu, G.; Lu, L.; Wu, Y.; Min, H.; Liu, J.; Wang, G. *J. Am. Chem. Soc.* **2006**, *128*, 12608–12609. (f) Wang, X. F.; Xu, J. B.; Zhang, B.; Yu, H. G.; Wang, J.; Zhang, X.; Yu, J. G.; Li, Q. *Adv. Mater.* **2006**, *18*, 2476–2480. (g) Liu, W. K.; Whitaker, K. M.; Kittilstved, K. R.; Gamelin, D. R. *J. Am. Chem. Soc.* **2006**, *128*, 3910–3911.

(3) Ba, J.; Fattakhova Rohlfing, D.; Feldhoff, A.; Brezesinski, T.; Djerdj, I.; Wark, M.; Niederberger, M. *Chem. Mater.* **2006**, *18*, 2848–2854.

(4) (a) Cabot, A.; Arbiol, J.; Morante, J. R.; Weimar, U.; Bârsan, N.; Göpel, W. *Sens. Actuators B* **2000**, *70*, 87–100. (b) Díaz, R.; Arbiol, J.; Cirera, A.; Sanz, F.; Peiró, F.; Cornet, A.; Morante, J. R. *Chem. Mater.* **2001**, *13*, 4362–4366. (c) Arbiol, J.; Cirera, A.; Peiró, F.; Cornet, A.; Morante, J. R.; Delgado, J. J.; Calvino, J. J. *Appl. Phys. Lett.* **2002**, *80*, 329–331. (d) Arbiol, J.; Cerdà, J.; Dezanneau, G.; Cirera, A.; Peiró, F.; Cornet, A.; Morante, J. R. *J. Appl. Phys.* **2002**, *92*, 853–861. (e) Díaz, R.; Arbiol, J.; Sanz, F.; Cornet, A.; Morante, J. R. *Chem. Mater.* **2002**, *14*, 3277–3283. (f) Ruiz, A. M.; Dezanneau, G.; Arbiol, J.; Cornet, A.; Morante, J. R. *Chem. Mater.* **2004**, *16*, 862–871. (g) Neri, G.; Bonavita, A.; Micali, G.; Rizzo, G.; Galvagno, S.; Niederberger, M.; Pinna, N. *Chem. Commun.* **2005**, *48*, 6032–6034.

(5) (a) Morrison, S. R. *Sens. Actuators* **1987**, *12*, 425–440. (b) Gentry, S. J.; Jones, T. A. *Sens. Actuators* **1986**, *10*, 141–163. (c) Yamazoe, N.; Kurokawa, Y.; Seiyama, T. *Sens. Actuators* **1983**, *4*, 283–289. (d) McAleer, J. F.; Moseley, P. T.; Norri, J. O. W.; Williams, D. E.; Tofield, B. C. *J. Chem. Soc. Faraday Trans* **1988**, *84*, 441–457. (e) Dieguez, A.; Vilà‘, A.; Cabot, A.; Romano-Rodriguez, A.; Morante, J. R.; Kappler, J.; Barsan, N.; Weimar, U.; Ğopel, W. *Sens. Actuators B* **2000**, *68*, 94–99.

(6) (a) Franke, M. E.; Koplin, T. J.; Simon, U. *Small* **2006**, *2*, 36–50. (b) Comini, E. *Anal. Chim. Acta* **2006**, *568*, 28–40. (c) Comini, E.; Faglia, G.; Sberveglieri, G.; Pan, Z.; Wang, Z. L *Appl. Phys. Lett.* **2002**, *81*, 1869–1871. (d) Kolmakov, A.; Zhang, Y.; Cheng, G.; Moskovits, M. *Adv. Mater.* **2003**, *15*, 997–1000. (e) Law, M.; Kind, H.; Messer, B.; Kim, F.; Yang, P. *Angew. Chem., Int. Ed.* **2002**, *41*, 2405–2408. (f) Liu, Y.; Liu, M. *Adv. Funct. Mater.* **2005**, *15*, 57–62. (g) Zhang, D.; Liu, Z.; Li, C.; Tang, T.; Liu, X.; Han, S.; Lei, B.; Zhou, C. *Nano Lett.* **2004**, *4*, 1919–1924.

(7) (a) Schweizer-Berberich, M.; Zheng, J. G.; Weimar, U.; Göpel, W.; Barsan, N.; Pentia, E.; Tomescu, A. *Sens. Actuators B* **1996**, *31*, 71. (b) Neri, G.; Bonavita, A.; Micali, G.; Donato, N.; Deorsola, F. A.; Mossino, P.; Amato, I.; De Benedetti, B. *Sens. Actuators B* **2006**, *117*, 196–204. (c) Menini, P.; Parret, F.; Guerrero, M.; Soulantica, K.; Erades, L.; Maisonnat, A.; Chaudret, B. *Sens. Actuators B* **2004**, *103*, 111–114. (d) Ruiz, A. M.; Cornet, A.; Shimanoe, K.; Morante, J. R.; Yamazoe, N. *Sens. Actuators B* **2005**, *108*, 34–40. (e) Cabot, A.; Dieguez, A.; Romano-Rodriguez, A.; Morante, J. R.; Barsan, N. *Sens. Actuators B* **2001**, *79*, 98–106. (f) Koziej, D.; Barsan, N.; Shimanoe, K.; Yamazoe, N.; Szuber, J.; Weimar, U. *Sens. Actuators B* **2006**, *118*, 98–104. (g) Erades, L.; Grandjean, D.; Nayral, C.; Soulantica, K.; Chaudret, B.; Menini, P.; Parret, F.; Maisonnat, A. *New J. Chem.* **2006**, *7*, 1026–1035. (h) Kolmakov, A.; Klenov, D. O.; Lilach, Y.; Stemmer, S.; Moskovits, M. *Nano Lett.* **2005**, *5*, 667–673.

(8) Epifani, M.; Díaz, R.; Arbiol, J.; Comini, E.; Sergent, N.; Pagnier, T.; Siciliano, P.; Faglia, G.; Morante, J. R. *Adv. Funct. Mater.* **2006**, *16*, 1488–1498.

(9) The (110) reflection at about 26.6°.

CG700970D